Using an Artificial Neural Network to Predict Flame Spread Across Electrical Wires

Lauren Gagnon[1]
Department of Mechanical Engineering,
University of California, Berkeley,
Hesse Hall,
Berkeley, CA 97420
e-mail: lauren_gagnon@berkeley.edu

Van P. Carey
Fellow ASME
Department of Mechanical Engineering,
University of California, Berkeley,
2521 Hearst Avenue, Etcheverry Hall,
Berkeley, CA 97420
e-mail: vpcarey@berkeley.edu

Carlos Fernandez-Pello
Fellow ASME
Department of Mechanical Engineering,
University of California, Berkeley,
Hesse Hall,
Berkeley, CA 97420
e-mail: ferpello@me.berkeley.edu

There is currently a global-scale transition from fossil fuel energy technologies toward increasing use of electrically driven energy technologies, especially transportation and heat, fueled by renewable energy sources, which is making fire safety in electrically powered systems increasingly important. The work presented here provides a coherent understanding of flame spread parametric trends and associated fire safety issues in electrical systems for structural, transportation, and space applications. This understanding was obtained through the use of an artificial neural network (ANN) that was trained to predict the flame spread rate along "laboratory" wires of different sizes and compositions (copper, nichrome, iron, and stainless-steel tube cores and HDPE, LDPE, and ETFE insulation sheaths) and exposed to different ambient conditions (varying flows, pressure, oxygen concentration, orientation, and gravitational strength). For these predictions, a comprehensive database of 1200 data points was created by incorporating flame spread rate results from both in-house experiments (400 data points) and external experiments from other sources (800 data points). The predictions from the ANN show that it is possible to merge various data sets, including results from horizontal, inclined, vertical, and microgravity experiments, and obtain unified predictive results. While these initial results are very encouraging with an overall average error rate of 14%, they also show that future improvements to the ANN could still be made to increase prediction accuracy.
[DOI: 10.1115/1.4050816]

Keywords: energy conversion/systems, energy systems analysis, renewable energy

1 Introduction

There is currently a global-scale transition from fossil fuel energy technologies toward increasing use of electrically driven energy technologies, especially transportation and heat, fueled by renewable energy sources [1]. Figure 1 [1] shows the required increase in electricity consumption for a renewable energy roadmap (REmap) from the present through 2050 that seeks to keep carbon emissions low enough such that the increase in global temperature is limited to 2 °C. This REmap map shows that there should be a doubling of electricity-produced energy consumption by 2050. Figure 2 [1] breaks this requirement down even further, showing that, for the REmap case, electricity-produced energy should account for one-third to one-half of consumption in industry and buildings and approximately one-third in transportation by the year 2050.

Such an expansion in the electricity demand is making fire safety in electrically powered systems increasingly important. The fire safety work here focuses specifically on the flammability of electrical wires, which are potential sources of fire ignition and spread in spacecrafts, aircrafts, vehicles, and structures [2–5]. The main focus of this work has previously been the potential for fires in spacecrafts, which can be originated by electrical wires and have disastrous consequences, especially since cabin environments for NASA's next generation of spacecrafts are planned to operate under reduced pressure and increased oxygen concentration conditions [6] to reduce space-walk preparation time.

However, considering the potential increase in demand for electricity on Earth, it is important to understand the burning behavior of electrical wires in their many different operating environments. Therefore, this work considers not only varying pressure, oxygen concentration, and gravitational strength, but also varying flow speed, wire orientation, and wire composition, which are import

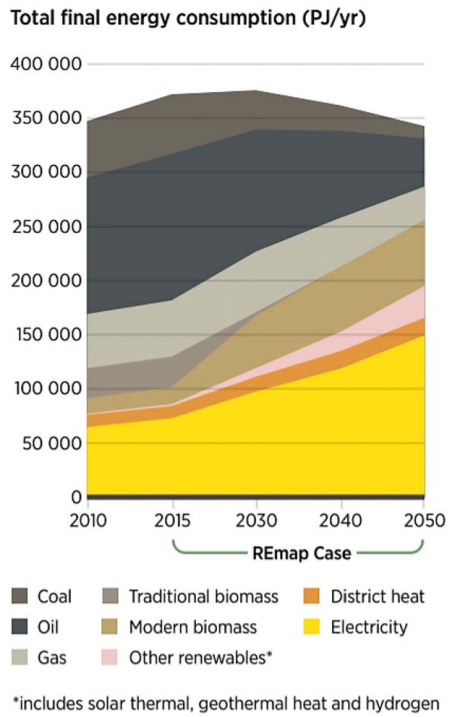

Fig. 1 The rising importance of electricity derived from renewable energy—share of electricity in total final energy consumption (PJ/year) (Reproduced with permission from Ref. [1]. Copyright 2018 by IRENA).

[1]Corresponding author.

Contributed by the Advanced Energy Systems Division of ASME for publication in the Journal of Energy Resources Technology. Manuscript received March 1, 2021; final manuscript received April 2, 2021; published online May 3, 2021. Assoc. Editor: Debjyoti Banerjee.

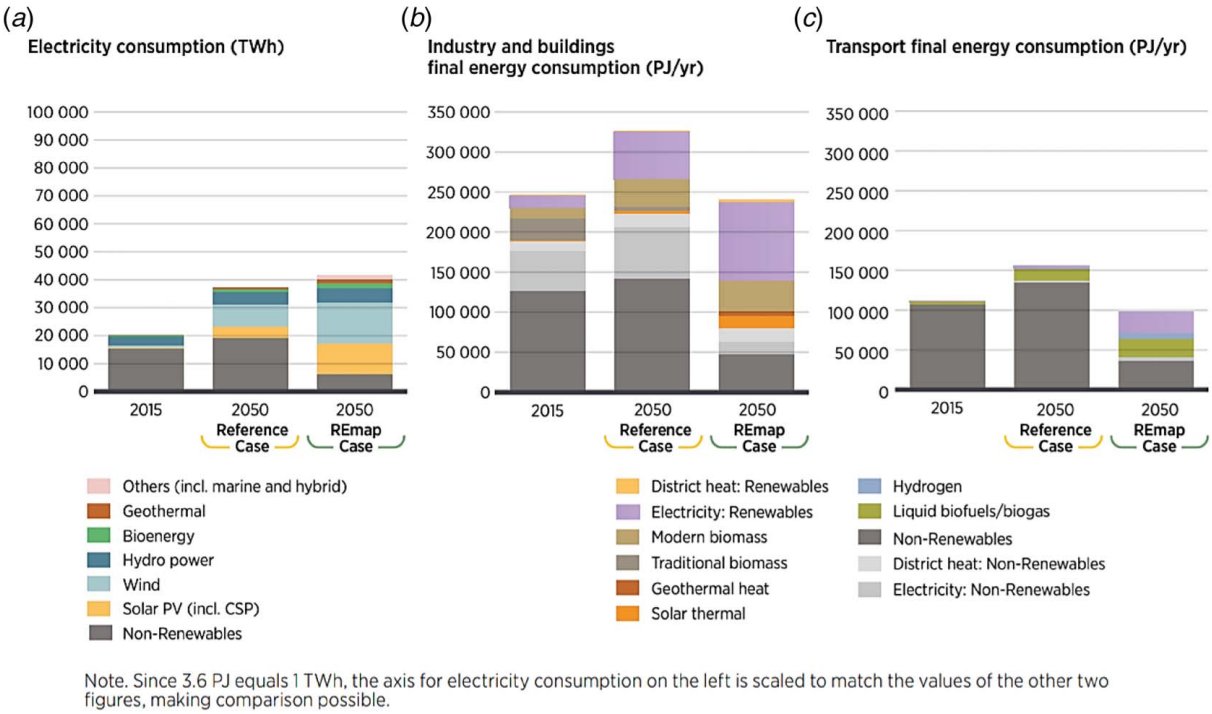

Fig. 2 Renewable energy should be scaled up to meet power, heat, and transport needs—(*a*) use of renewable and fossil energy in electricity generation, (*b*) buildings and industry, and (*c*) transport—reference and REmap cases, 2015–2050 (TWh/year or PJ/year) (Reproduced with permission from Ref. [1]. Copyright 2018 by IRENA).

parameters in nearly every different wire environment, including the aforementioned aircraft, vehicle, and structural applications.

2 Previous Findings

The main burning mechanism this work uses to assess the flammability of wire insulation materials is flame spread rate because after the material is ignited, the rate of heat released by the fire is dependent on its rate of spread. While there have been many previous studies which analyzed analytical solutions to the flame spread rate along electrical wire problem, two of the most commonly cited models [7–12], shown in Eqs. (1) and (2) (see Nomenclature for variable definitions), are derived simply from the fundamentals of flame spread [13,14] and have shown varying success in their prediction capabilities, especially when variables such as forced flow, pressure, oxygen concentration, gravitational strength, and wire inclination deviate from the standard.

$$v_f = \frac{\dot{q}''_f l_f + \dot{q}''_c l_c + \dot{q}''_m l_m - \dot{q}''_{s,r} l_h}{\rho_i c_i \delta_i (T_{py} - T_\infty)} \tag{1}$$

$$v_f = \frac{\dot{Q}_{f\to i} + \dot{Q}_{c\to i}}{(A_i \rho_i c_{p,i} + A_c \rho_c c_{p,c})(T_{py} - T_\infty)} \tag{2}$$

Other flame spread rate equations have been explored [15–17], and still, others have attempted to expand on the problem to account for parameters such as wire inclination [18,19] and electrical current [19,20]. However, there has yet to be found an all-encompassing equation for the flame spread rate along the electrical wire problem. While the current work does not attempt to find such an equation, it does, for the first time in this field, bring together and unify the current existing database of flame spread rate data along electrical wires from the available works, including those from Fang et al. [15,21], Fujita et at. [22], Gagnon et al. [23], Hu et al. [18,24], Kikuchi et al. [25], Kobayashi et al. [7,8], Konno et al. [9,26,27], Lim et al. [28], Lu et al. [10,29], Ma et al. [11], Miyamoto et al. [12], Nagachi et al. [30], Nakamura et al. [31–33], Takahashi et al. [34], Wang et al. [16,20], and Zhao et al. [17,19] as well as some previously unpublished, in-house data. Altogether, the database used for analysis in this study consisted of approximately 1200 data points, with approximately one-third (400) coming from internal experiments and two-thirds (800) coming from external sources. This information is provided in more detail in Table 1.

3 Prediction Methods—Artificial Neural Network

To create a model of this comprehensive database, an artificial neural network (ANN) was trained to predict the flame spread rate along wires of different sizes and compositions. Tests from all sources in the database were conducted with "laboratory" wires consisting of metal cores and plastic insulation sheaths. The represented core materials include copper, nichrome, iron, and stainless-steel tubing with diameters ranging from 0.30 mm (0.012 in.) to 5.5 mm (0.23 in.), and the represented plastic insulation materials include two different types of polyethylene (PE), high-density polyethylene (HDPE), and low-density polyethylene (LDPE), and ethylene tetraflouroethylene (ETFE) with thicknesses ranging from 0.075 mm (0.0030 in.) to 2.3 mm (0.091 in.). An example of such a "laboratory" wire is shown in Fig. 3 [23]. The relative simplicity of the "laboratory" wires, while not intended to necessarily reproduce actual electrical wires, are conventionally used to facilitate the interpretation of experimental results and to compare results with other experiments being conducted in the field.

During testing, wires were also exposed to different ambient conditions, including varying flows, pressure, oxygen concentration, orientation, and gravitational strength. Flow velocities ranged from 3.5 m/s (11 ft/s) opposed to the flame spread direction to 6.8 m/s (22 ft/s) concurrent to the flame spread direction; ambient pressures ranged from 10 kPa (1.5 psi) to 1000 kPa (145 psi); ambient oxygen concentrations ranged from 14% to 50%; wire orientation/inclination ranged from horizontal to vertical, and gravitational strengths ranged from 10^{-5} g to 1 g. These ranges of environmental parameters as well as wire sizes and compositions are summarized in Table 2.

It should be noted that some references from which data were gathered for use in the comprehensive flame spread rate along

Table 1 Summary of references used to create flame spread rate over electrical wire database

1st Author, Year, Ref #	Core Mat'l	Ins. Mat'l	d_c (mm)	τ (mm)	v (m/s)	g (g's)	$\%O_2$	P (kPa)	Wire orientation	Data points
Fang, 2020 [15]	NiCr	ETFE, PE	0.50	0.15	0.0	1	Varied	Varied	Horizontal	30
Fang, 2019 [21]	Cu, NiCr	PE	0.50	0.15	0.0	1	Varied	Varied	Horizontal	47
Fujita, 2002 [22]	NiCr	PE	0.50	Varied	Varied	10^{-5}	Varied	101	–	31
Gagnon, 2020 [23]	Cu	LDPE	0.64	1.7	Varied	1	21	Varied	Horizontal	46
Gagnon	Varied	LDPE	Varied	Varied	Varied	1	Varied	Varied	Horizontal	319
Hu, 2015 [18]	Cu	PE	Varied	Varied	0.0	1	21	Varied	Varied	80
Hu, 2019 [24]	Cu, NiCr	PE	Varied	Varied	0.0	1	21	Varied	Horizontal	40
Kikuchi, 1998 [25]	Cu	ETFE	0.32	0.25	0.0	Varied	Varied	101	Horizontal	9
Kobayashi, 2018 [7]	Cu, steel	HDPE, LDPE	Varied	Varied	Varied	1	Varied	101	Varied	123
Kobayashi, 2020 [8]	Cu, steel	LDPE	2.5	0.75	0.0	1	21	varied	Horizontal	20
Konno, 2019 [9]	Cu, NiCr	LDPE	0.50	0.15	−0.15	1	varied	101	Vertical	25
Konno, 2020 [26]	Cu	LDPE	Varied	Varied	−0.10	0.03	Varied	101	Vertical	10
Konno, 2020 [27]	Varied	LDPE	0.50	0.15	−0.04	1	Varied	101	Vertical	30
Lim, 2017 [28]	NiCr	PE	0.50	0.15	0.0	1	21	101	Varied	17
Lu, 2019 [10]	Cu	PE	Varied	Varied	Varied	1	21	101	Horizontal	36
Lu, 2019 [29]	Cu	PE	0.50	0.15	Varied	1	21	101	Varied	48
Ma, 2020 [11]	Cu, NiCr	PE	Varied	Varied	Varied	1	21	101	Horizontal	82
Miyamoto, 2016 [12]	Cu, steel	HDPE, LDPE	Varied	Varied	−0.04	1	Varied	101	Vertical	20
Nagachi, 2019 [30]	Cu, NiCr	PE	0.50	0.30	Varied	0.01	Varied	101	–	30
Nakamura, 2008, [31]	NiCr	PE	0.50	0.15	0.0	1	21	Varied	Horizontal	6
Nakamura, 2008 [32]	Fe, NiCr	PE	0.50	0.15	Varied	1	21	Varied	Horizontal	34
Nakamura, 2009 [33]	Fe, NiCr	PE	0.50	0.15	0.0	1	21	Varied	Horizontal	16
Takahashi, 2013 [34]	NiCr	LDPE	0.50	0.15	Varied	0.01	17	101	–	4
Wang, 2020 [16]	Cu	PE	Varied	Varied	0.0	1	21	Varied	Horizontal	12
Wang, 2020 [20]	Cu, NiCr	PE	0.80	0.15	0.0	1	21	Varied	Horizontal	15
Zhao, 2017 [17]	Cu	PE	0.48	0.50	0.0	1	21	Varied	Horizontal	11
Zhao, 2020 [19]	Cu	PE	0.50	0.15	0.0	1	21	101	Varied	11

electrical wire database included other experimental parameters, such as dilution gas [25], external radiation [12,26], or electric fields [20,28,34]. While those parameters are highly important to the wire flame spread rate problem, there were either too few data points or too much variation in experimental design for the current analysis; therefore, any experimental data with parameters in addition to the ones listed above were excluded.

The way in which this amalgamated data set was used in conjunction with the ANN is shown in Fig. 4, which depicts the full procedure of data preparation, then training of the ANN, and finally validation of the ANN. The first stage, data preparation, which includes all boxes in Fig. 4 that are touching the black arrows, involves transforming the data corresponding to the input parameters, listed in Table 3, as well as experimentally gathered output data, in this case, flame spread rate, into normalized values. This calculation is carried out by taking each data point of a specific parameter and dividing it by the corresponding mean of that parameter. The result of this normalization allows the input data to both be dimensionless and closer to unity, putting each parameter on the same order of magnitude.

Next, half of these data is taken for use in training the ANN, while the remaining half is reserved for the validation of the ANN. The form of the ANN that was trained to predict flame spread rate along electrical wires is shown in Fig. 5, with the input parameters again defined in Table 3. The basics of the ANN training can first be thought of in terms of a single node, several of which are depicted in Fig. 5. Each of these nodes is in a position (i,j) and takes in various inputs ($x_{i,j,in}$), multiplies them by weights ($w_{i,j,k}$), linearly combines those products along with a bias value ($b_{i,j}$), and inputs the result ($z_{i,j}$) into an activation function (σ) to determine the node output ($x_{i,j,out}$). This calculation is then carried out for all nodes in the ANN which are typically arranged in layers, as shown in Fig. 5, so the outputs from every node in one layer become the inputs for each node in the next. Once the calculations have been iterated through the entire ANN, one epoch is considered to have passed. This process can then be repeated for multiple epochs with the weights and biases being adjusted each time through backpropagation to refine the ANN output, leading to more accurate predictions. Further description of the fundamentals of how an ANN works is explained by Kröse and Smagt [35], the details of which will not be covered here.

The basic structure of the ANN utilized here was created with the open-source python package, Keras [36]. The input layer consists of 15 nodes, corresponding to the 12 selected input parameters, two of which were vectors with multiple components, with each assigned

Fig. 3 Example wire sample with (left) core length of 125 mm (4.9 in.) and LDPE insulation length of 100 mm (3.9 in.) and (right) 0.64 mm (0.025 in) diameter copper core and LDPE insulation with 4 mm (0.16 in.) outer diameter [23]

Table 2 Wire material properties and sizes and environmental parameters spanned by the flame spread rate over electrical wire database

Parameter	Minimum value	Maximum value
ρ_c	7800 kg/m^3 (NiCr)	8880 kg/m^3 (Cu)
k_c	17.4 W/m·K (steel)	398 W/m·K (Cu)
$c_{p,c}$	390 J/kg·K (Cu)	500 J/kg·K (steel)
d_c	0.30 mm	5.5 mm
A_c	0.071 mm^2	24 mm^2
ρ_i	923 kg/m^3 (LDPE)	1700 kg/m^3 (ETFE)
k_i	0.238 W/m·K (ETFE)	0.338 W/m·K (HDPE)
$c_{p,i}$	1800 J/kg·K (ETFE)	2075 J/kg·K (HDPE)
τ	0.075 mm	2.3 mm
A_i	0.14 mm^2	40.6 mm^2
$\%O_2$	14%	50%
P	10 kPa	1000 kPa
$\overline{v}$	−3.5 m/s	6.8 m/s
$\overline{g}$	10^{-5} g	1 g

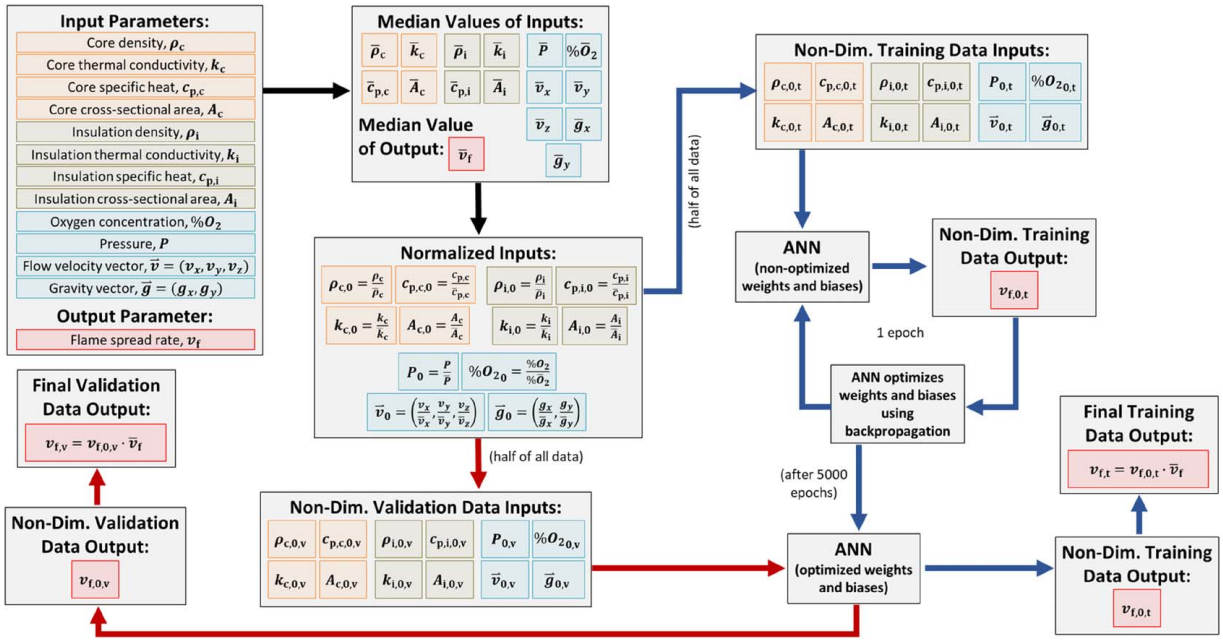

Fig. 4 Flowchart of data preparation (first three boxes), then ANN training (the seven boxes on the right), and finally ANN validation (remaining three boxes and optimized ANN box)

its own node. Figure 5 is depicted as having 12 input nodes for simplicity. Based on the number of input parameters, it was determined that two dense hidden layers with 12 nodes each should be used (again, Fig. 5 is depicted with 9 for simplicity), which are appropriately sized to ensure that the ANN would not be over-trained and begin to memorize the data [37–39]. Finally, the output layer consists of only one node, corresponding to the single output parameter of interest, the flame spread rate.

The chosen activation function was a hyperbolic tangent because it more easily dealt with positive and negative input parameters present in both the velocity and gravitational strength vectors. Finally, the weight and bias values were refined over approximately 5000 epochs using the root-mean-square propagation (RMSprop) function, a popular gradient descent optimization algorithm which is reliable and fast in deep learning networks [40], within the Keras package.

After training takes place, validation of the ANN is carried out using the reserved half of the data that were not put through the training process. Because the ANN has never seen this data before, it is able to validate the training of the ANN and show that it is actually able to make predictions and has not just memorized the patterns found in the training data. The results from the validation dataset are obtained by running the corresponding input parameters through the fully trained ANN for one epoch.

Table 3 List of input parameters used in the ANN

Input parameter name	Input parameter symbol
Wire core density	ρ_c
Wire core thermal conductivity	k_c
Wire core specific heat	$c_{p,c}$
Wire core cross-sectional area	A_c
Wire insulation density	ρ_i
Wire insulation thermal conductivity	k_i
Wire insulation specific heat	$c_{p,i}$
Wire insulation cross-sectional area	A_i
Oxygen concentration	$\%O_2$
Pressure	P
Flow velocity vector	$\vec{v} = (v_x, v_y, v_z)$
Gravitational strength vector	$\vec{g} = (g_x, g_y)$

4 Results and Discussion

4.1 Validation and Training Data. Figure 6 provides the results from the ANN's training and shows a very strong agreement between the ANN's predictions and the experimentally measured values, with an average error of 12%. However, it is expected to see good agreement here, as these are the data that were used to train the ANN. The true indication of the ANN's performance is revealed by the validation results, which will be the focus of this section of the discussion from this point onward.

Figure 7 provides the results of the ANN's validation with data sets divided by reference origin. Again, a strong agreement is observed between the ANN's predictions and the experimentally measured values, with an average error of 16% for data the ANN had never encountered before. Such results show that a comprehensive model of the available data in the field is possible to obtain.

Figures 8 and 9 shed further light on the results by separating the ANN's validation results into categories based on wire orientation and showing definitive proof that the wire flame spread problem that is so often investigated separately based on wire orientation and the strength of the gravity can actually be viewed as one unified problem. The same could be said for opposed and concurrent flame spread, which are also both represented in the ANN results as well. This is an important result of the ANN application since it simplifies the way that flame spread has been traditionally studied and extends the concept that flame spread can be analyzed in a unified manner, as proposed by Fernandez-Pello and Mao [41] for concurrent flame spread, to other flame spread configurations.

Such strong agreement indicates that the selected input parameters of core and insulation densities, thermal conductivities, specific heats, and cross-sectional areas, oxygen concentration, pressure, flow velocity, and gravitational strength are all highly important to the wire flame spread problem. However, these results also show that there is great room for improvement in the ANN predictions.

4.2 Analysis of Outliers. While most of the predictions given by the ANN's validation results show good agreement with the measured values, there are two data points in Figs. 7 and 8 that stand out from the rest, with much higher predictions for flame spread rate produced by the ANN than were measured

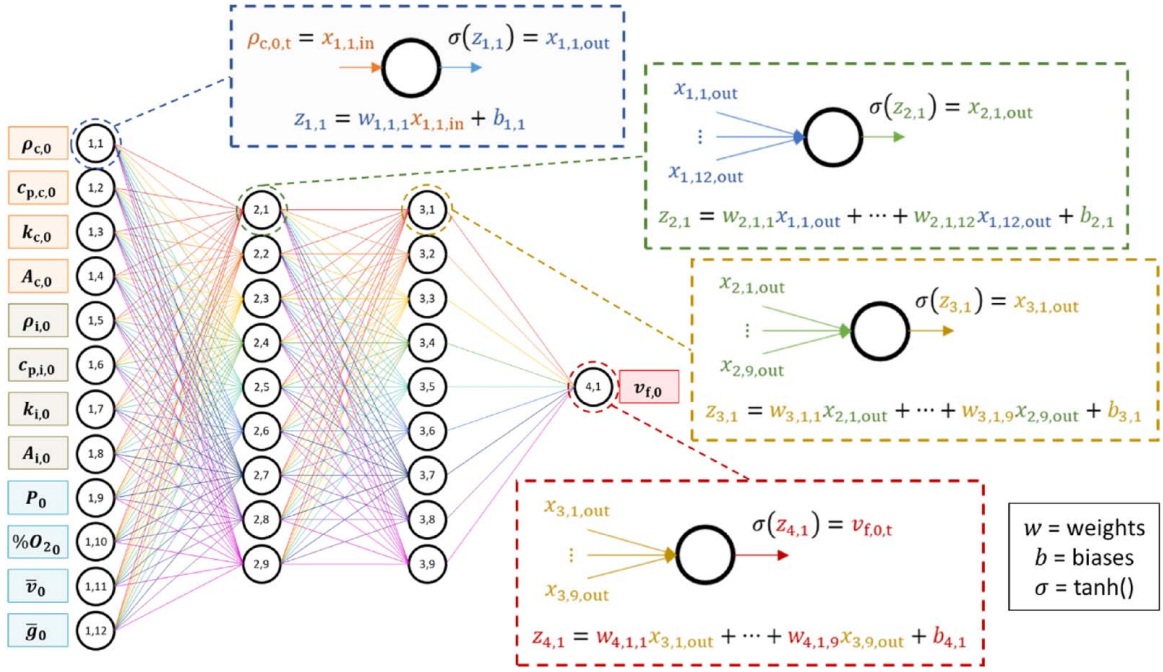

Fig. 5 Visual representation of ANN used to predict flame spread rate across electrical wires

experimentally. It is currently unknown why these two data points in particular show such poor agreement between the measured and predicted values. Because these data points fall on the higher side of flame spread rate values, the first thought may be to assume that perhaps these data points represent experimental conditions that were unlike any ANN had encountered before, and thus resulted in poor predictions. However, each of the input parameters for these data points falls well within the ranges previously cited for this data set in Table 2.

While it is possible that experimental errors could have been made for these particular data points, this disagreement between the measured values and the ANN predicted values of flame spread rate in conjunction with the average 16% error rate is more likely indicating that there may be other input parameters necessary for the ANN to produce more accurate results.

One such input parameter may be more specific values for insulation material/thermal properties. While many of the data sources utilized some form of PE as the insulation, the precise type, HDPE or LDPE, was not always indicated, and specifications of the material properties were not always provided. As well, even when the type of PE was indicated and material properties were provided, there was a significant range in cited properties, even among the same type of PE. For example, densities cited for LDPE ranged from 920 kg/m^3 (57.4 lb/ft^3) to 940 kg/m^3 (58.7 lb/ft^3), and

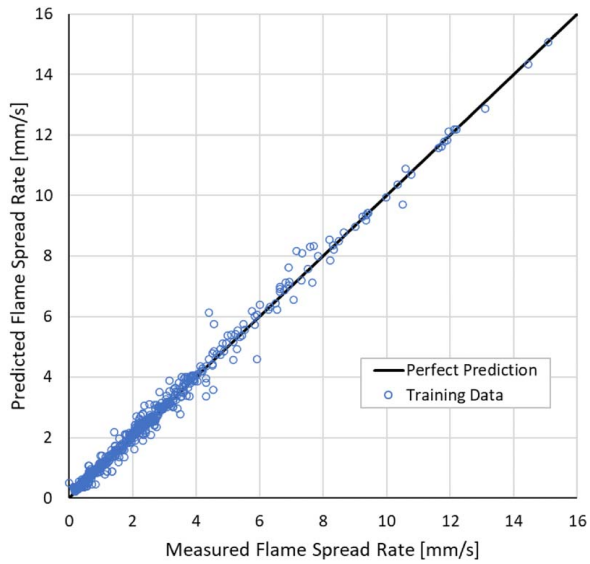

Fig. 6 ANN training results comparing ANN predicted flame spread rate and experimentally measured flame spread rate

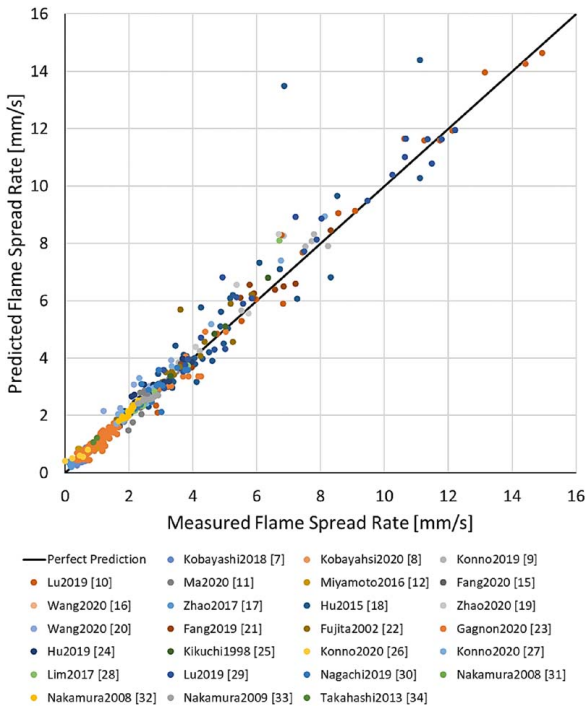

Fig. 7 ANN validation results comparing ANN predicted flame spread rate and experimentally measured flame spread rate with data sets distinguished by reference origin

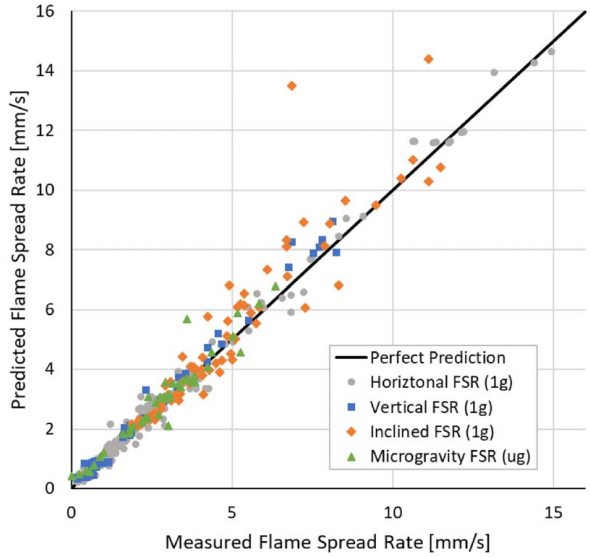

Fig. 8 ANN validation results comparing ANN predicted flame spread rate and experimentally measured flame spread rate with data sets distinguished by wire orientation

densities cited for HDPE ranged from 944 kg/m^3 (58.9 lb/ft^3) to 959 kg/m^3 (59.9 lb/ft^3). Due to such variation and without cited values from each source, averages of the material/thermal properties for each insulation type were utilized as input parameters. As well, through necessity, whenever the insulation material was listed as PE with no material properties provided, it was assumed that it was of the low-density variety, as that is the more popular material of choice in the field. Since LDPE and HDPE have such different behavior during flame spread along their surfaces, particularly regarding melting and dripping, it is probable that with more precision in these parameters, the ANN's predictions could improve.

Looking at Eqs. (1) and (2), another obvious and easily measured input parameter can be identified: the temperature difference between pyrolysis temperature of the insulation and ambient temperature. Unfortunately, this is another situation of poorly cited information, with few sources providing data on ambient temperature during experiments or pyrolysis temperature for their specific insulation material.

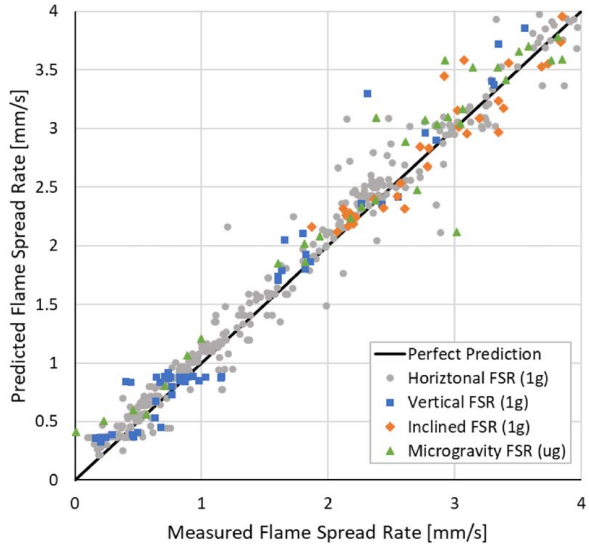

Fig. 9 ANN validation results comparing ANN predicted flame spread rate and experimentally measured flame spread rate focusing on the majority of results which fall between 0 and 4 mm/s (0.16 in./s) with data sets distinguished by wire orientation

4.3 Parametric Trends. While there is definitely room for improvement in the ANN model, that is not to say that nothing further can be learned from it in its current state. Examining some of the parametric trends predicted by the ANN can give further insight into the flame spread rate along the electrical wire insulation problem. Because of the previous focus on spacecraft applications as well as the current focus on terrestrial transportation and structural applications, several parametric trends were examined.

For the more spacecraft-related applications as well as limited terrestrial applications, Fig. 10 shows a parametric surface which demonstrates the ANN's predictions for flame spread rate's dependence on oxygen concentration and ambient pressure, spanning both the oxygen concentration and pressure ranges of the gathered data set, when all other variables are held constant (mid-sized copper core diameter of 2.9 mm (0.11 in.), mid-thickness LDPE insulation of 1.2 mm (0.047 in.), no forced flow, horizontally oriented wire, and 1 g gravitational strength).

The surface clearly displays the well-known trend for flame spread rate to increase with both increasing oxygen concentration and increasing pressure. However, Fig. 10 also shows further nuances of the problem which have not previously been well explored, such as the response of flame spread rate to high oxygen concentrations at low pressures as well as its response to high pressures at low oxygen concentrations. The ANN's predictions show that these parameters somewhat balance each other out and that even at extremely low oxygen concentrations or pressures, a high value of the other parameter can still result in a moderately fast flame spread rate.

Aiming for further relevance to terrestrial transportation and structural applications, Fig. 11 shows a parametric surface which demonstrates the ANN's predictions for flame spread rate's dependence on copper wire core cross-sectional area and axial flow velocity, spanning both the wire core diameter and axial flow velocity ranges of the gathered data set with all other variables held at the same previous constants, and this time with 21% oxygen concentration and 101 kPa (14.6 psi) ambient pressure. This figure shows that there is much more variation in flame spread rate when varying core cross-sectional area and axial flow velocity, suggesting that these parameters may be highly important for assessing fire safety.

As well, one extremely interesting feature that is found in Fig. 11 is the steep drop off in flame spread rate when the cross-sectional area of the core approaches ~10 mm^2 (0.016 in^2), with some

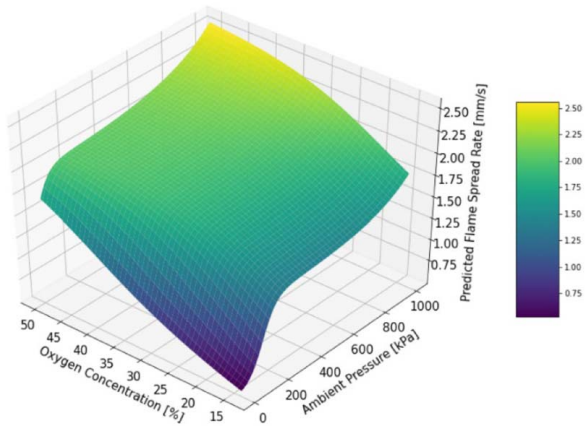

Fig. 10 Parametric surface showing flame spread rate dependence on ambient oxygen concentration and pressure with constant copper wire core of 2.9 mm (0.11 in.) diameter, LDPE insulation of 1.2 mm (0.047 in.) thickness, no forced flow, horizontally oriented wire, and 1 g gravitational strength

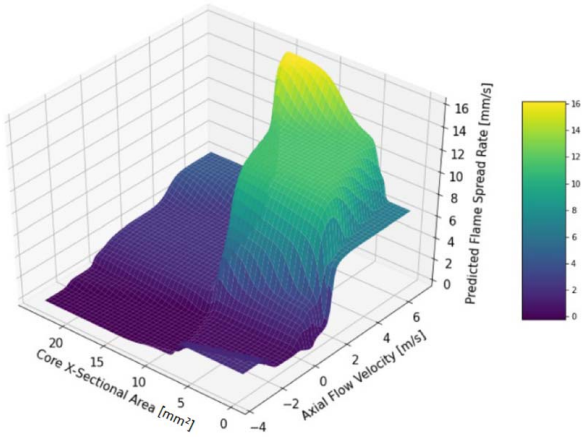

Fig. 11 Parametric surface showing flame spread rate dependence on cross-sectional area of copper wire core and axial flow velocity with constant LDPE insulation of 1.2 mm (0.047 in) thickness, 21% ambient oxygen concentration, 101 kPa (14.6 psi) ambient pressure, horizontally oriented wire, and 1 g gravitational strength

slight variation depending on the axial flow velocity. This dramatic decrease in flame spread rate may illustrate a critical core diameter, where the wire core transitions from being a source conducting heat toward the flame to a sink drawing heat out of it. Interestingly, this effect does not seem to be nearly as present in the opposed flow (negative axial flow velocity) regime.

5 Future Work

The initial results from the ANN have shown to be very promising, and it is believed that the ANN could be used for much more in-depth analyses in the future. To begin with, only a very few number of flame spread rate parametric surfaces were examined in this study. Analysis of all the other possible flame spread rate parametric surfaces could bring so much further insight into the flame spread rate along electrical wire problem and potentially reveal results or nuances that have previously gone undiscovered.

A sensitivity analysis examining each of the parameters affecting the flame spread rate along the electrical wire insulation problem could also be performed using the predictions of the ANN. Such an analysis could be an immensely useful tool for shedding further light on which parameters in the problem are the most important and influential when it comes to flame spread rate and assessing fire safety.

Finally, the ANN could be expanded to include further parameters. As mentioned previously, some variables such as electric fields or electric currents and external radiation were excluded from this analysis. However, adapting the comprehensive database and the ANN to account for these variables could make the ANN predictions even more comprehensive and relevant to the current applications as well as additional ones.

6 Conclusion

The flame spread rate along electrical wire insulation problem is highly complex and can encompass many variables, including wire core and insulation material/thermal properties, oxygen concentration, pressure, flow velocity, wire orientation, and gravitational strength. With the current global-scale transition from fossil fuel energy technologies toward increasing use of electrically driven energy technologies and a resulting potential for electricity-produced energy consumption to double over the coming decades, it is highly important to further the understanding of electrical wire flammability, which was examined here through analysis of flame spread rate. While there have been numerous past studies that have looked at this flame spread rate problem, there has yet to be one cohesive analysis of the problem as a whole.

By combining data sets from a multitude of sources at a scale that has never been done before and training an artificial neural network to predict flame spread rates across various types of electrical wires under many different ambient conditions, for the first time ever, comprehensive results showed that it is possible to unify this wire flame spread problem. With an average error of 12% from the ANN's training results and 16% from the ANN's validation results, great potential is shown by the ANN to provide a comprehensive model of this problem.

Analysis of parametric surfaces developed from the predictions of the ANN showed many nuances in the flame spread rate's dependence on various parameters. By examining the effects of oxygen concentration and pressure, their interactions with one another to balance flame spread rate could be seen. Looking at the influence of wire core cross-sectional area and axial flow velocity on flame spread rate showed there is a possible clear cutoff for a critical core diameter in which the wire core goes from acting as a heat source to a heat sink to the flame.

While the initial results from the ANN are exceedingly promising, it must be remembered that there are also still improvements that can be made to the ANN to increase the accuracy of its predictions. With further training using a wider variety and more accurate input data as well as greater insight into influential parameters, predictions may become even better with future iterations of the ANN.

Acknowledgment

The authors would like to thank Yusuke Konno and Professor Osamu Fujita for providing the authors with the wire samples used to conduct their experiments. The authors would also like to acknowledge Dr. Sandra Olson for her advice on the work and comments on the study.

Conflict of Interest

There are no conflicts of interest.

Data Availability Statement

The data sets generated and supporting the findings of this article are obtainable from the corresponding author upon reasonable request.

Funding Data

- National Aeronautics and Space Administration (NASA) (Grant No. 80NSSC19K0331).

Nomenclature

- b = ANN biases (subscripts i and j appear, indicating node location)
- g = gravitational strength vector component (subscripts x and y appear, indicating direction)
- k = thermal conductivity (subscripts of i and c appear, indicating insulation and core, respectively)
- l = heated length (subscripts of f, c, m, and h appear, indicating flame, core, melted insulation, and maximum heated length, respectively)
- v = Flow velocity vector component (subscripts x, y, and z appear, indicating direction)
- w = ANN weights (subscripts i and j appear, indicating node location; subscript k appears, indicating j position of node input)

x = ANN node inputs/outputs (subscripts i and j, appear, indicating node position; subscripts *in* and *out* appear, indicating node input or output)
z = ANN intermediate calculation (subscripts i and j appear, indicating node location)
A = cross-sectional area (subscripts of i and c appear, indicating insulation and core, respectively)
P = pressure
$\vec{g}$ = gravitational strength vector
$\vec{v}$ = Flow velocity vector
$\dot{q}''$ = heat flux (subscripts of f, c, m, and s,r appear, indicating flame, core, melted insulation, and surface re-radiation, respectively)
c_p = specific heat (subscripts of i and c appear, indicating insulation and core, respectively)
d_c = wire core diameter
v_f = flame spread rate
T_{py} = pyrolysis temperature of insulation
T_∞ = ambient temperature
$\dot{Q}_{f\to i}$ = heat conduction from the flame to the insulation
$\dot{Q}_{c\to i}$ = heat conduction from the core to the insulation
δ_i = insulation thickness
ρ = density (subscripts of i and c appear, indicating insulation and core, respectively)
σ = ANN activation function, defined as tanh for the current study
τ = insulation thickness
$\%O_2$ = percent oxygen concentration

References

[1] IRENA, 2018, *Global Energy Transformation: A Roadmap to 2050*, International Renewable Energy Agency, Abu Dhabi.
[2] Babrauskas, V., 2003, *Ignition Handbook*, Fire Science Publishers.
[3] U.S. Department of Homeland Security, 2010, *Residential Building Electrical Malfunction Fire Trends*, FEMA, Emmitsburg, MA.
[4] Ahrens, M., 2016, Home Structure Fires, NFPA.
[5] Fernandez-Pello, A., Hasegawa, H., Staggs, K., Lipska-quinn, A., and Alvares, N., 1991, "A Study of the Fire Performance of Electrical Cables," Fire Safety Science, **3**, pp. 237–247.
[6] Lange, K. E., Perka, A. T., Duffield, B. E., Duffield, B. E., and Jeng, F. F., 2005, *Bounding the Spacecraft Atmosphere Design Space for Future Exploration Missions*, NASA, Houston, TX.
[7] Kobayashi, Y., Konno, Y., Huang, X., Nakaya, S., Tsue, M., Hashimoto, N., Fujita, O., and Fernandez-Pello, C., 2018, "Effect of Insulation Melting and Dripping on Opposed Flame Spread Over Laboratory Simulated Electrical Wires," Fire Saf. J., **95**, pp. 1–10.
[8] Kobayashi, Y., Nakaya, S., Tsue, M., and Takahashi, S., 2021, "Flame Spread Over Polyethylene-Insulated Copper and Stainless-Steel Wires at High Pressure," Fire Saf. J., **120**.
[9] Konno, Y., Hashimoto, N., and Fujita, O., 2019, "Downward Flame Spreading Over Electric Wire Under Various Oxygen Concentrations," Proc. Combust. Inst., **37**(3), pp. 3817–3824.
[10] Lu, Y., Hu, L., Huang, X., and Fernandez-Pello, C., 2019, "Concurrent Flame Spread and Blow-Off Over Horizontal Thin Electrical Wires," Fire Technol., **55**(1), pp. 193–209.
[11] Ma, Y., Zhang, X., Lu, Y., Lv, J., Zhu, N., and Hu, L., 2020, "Effect of Transverse Flow on Flame Spread and Extinction Over Polyethylene-Insulated Wires," Proc. Combust. Inst., **38**(3), pp. 4727–4735.
[12] Miyamoto, K., Huang, X., Hashimoto, N., Osamu, F., and Fernandez-Pello, C., 2016, "Opposed Flame Spread Over Polyethylene Insulated Wires Under Varying External Radiations and Oxygen Concentrations," Proceedings of 46th International Conference on Environmental Systems, Vienna, Austria, July 10–14.
[13] Quintiere, J. G., 2006, *Fundamentals of Fire Phenomena*, John Wiley & Sons, Ltd., New York.
[14] Fernandez-Pello, A. C., 1995, "The Solid Phase," Combustion Fundamentals of Fire, pp. 31–100.
[15] Fang, J., Xue, Y., Wang, J., He, X., Zhang, Y., Zhao, S., and Zhang, Y., 2020, "PE and ETFE Wire Insulation Flame Morphologies and Spread Rates Under Subatmospheric Pressures," J. Thermoplast. Compos. Mater.
[16] Wang, Z., and Wang, J., 2020, "Experimental Study on Flame Propagation Over Horizontal Electrical Wires Under Varying Pressure," Int. J. Therm. Sci., **156**.
[17] Zhao, Y., Chen, J., Chen, X., and Lu, S., 2017, "Pressure Effect on Flame Spread Over Polyethylene-Insulated Copper Core Wire," Appl. Therm. Eng., **123**, pp. 1042–1049.
[18] Hu, L., Zhang, Y., Yoshioka, K., Izumo, H., and Fujita, O., 2015, "Flame Spread Over Electric Wire With High Thermal Conductivity Metal Core at Different Inclinations," Proc. Combust. Inst., **35**(3), pp. 2607–2614.
[19] Zhao, L., Zhang, Q., Tu, R., Fang, J., Wang, J., and Zhang, Y., 2020, "Effects of Electric Current and Sample Orientation of Flame Spread Over Electrical Wires," Fire Saf. J., **112**.
[20] Wang, Z., Zhou, T., Wei, R., and Wang, J., 2020, "Experimental Study of Flame Spread Over PE-Insulated Single Copper Core Wire Under Varying Pressure and Electric Current," Fire Mater., **44**(6), pp. 835–843.
[21] Fang, J., Zhang, Y., Huang, X., Xue, Y., Want, J., Zhao, S., He, X., and Zhao, L., 2019, "Dripping and Fire Extinction Limits of Thin Wire: Effect of Pressure and Oxygen," Combust. Sci. Technol., **193**(3), pp. 437–452.
[22] Fujita, O., Nishizawa, K., and Ito, K., 2002, "Effect of Low External Flow on Flame Spread Over Polyethylene-Insulated Wire in Microgravity," Proc. Combust. Inst., **29**(2), pp. 2545–2552.
[23] Gagnon, L., Fernandez-Pello, C., Urban, J. L., Carey, V. P., Konno, Y., and Fujita, O., 2020, "Effect of Reduced Ambient Pressures and Opposed Airflows on the Flame," Fire Saf. J., **120**.
[24] Hu, L., Zhu, K., Lu, Y., and Zhang, X., 2019, "An Experimental Study on Flame Spread Over Electrical Wire with High Conductivity Copper Core and Controlling Heat Transfer Mechanism Under Sub-atmospheric Pressures," Int. J. Therm. Sci., **141**, pp. 141–149.
[25] Kikuchi, M., Fujita, O., Ito, K., Sato, A., and Sakuraya, T., 1998, "Experimental Study on Flame Spread Over Wire Insulation in Microgravity," Symp. (Int.) Combust., **27**(2), pp. 2507–2514.
[26] Konno, Y., Kobayashi, Y., Fernandez-Pello, C., Hashimoto, N., Nakaya, S., Tsue, M., and Fujita, O., 2020, "Opposed-Flow Flame Spread and Extinction in Electric Wires: The Effects of Gravity, External Radiant Heat Flux, and Wire Characteristics on Wire Flammability," Fire Technol., **56**(1), pp. 131–148.
[27] Konno, Y., Hashimoto, N., and Fujita, O., 2020, "Role of Wire Core in Extinction of Opposed Flame Spread Over Thin Electric Wires," Combust. Flame, **220**, pp. 7–15.
[28] Lim, S. J., Park, S. H., Park, J., Fujita, O., Keel, S. I., and Chung, H. S., 2017, "Flame Spread Over Inclined Electrical Wires With AC Electric Fields," Combust. Flame, **185**, pp. 82–92.
[29] Lu, Y., Huang, X., Hu, L., and Fernandez-Pello, C., 2019, "The Interaction Between Fuel Inclination and Horizontal Wind: Experimental Study Using Thin Wire," Proc. Combust. Inst., **37**(3), pp. 3809–3816.
[30] Nagachi, M., Mitsui, F., Citerne, J.-M., Dutilleul, H., Guibaud, A., Jomaas, G., Legros, G., Hashimoto, N., and Fujita, O., 2019, "Can a Spreading Flame Over Electric Wire Insulation in Concurrent Flow Achieve Steady Propagation in Microgravity?," Proc. Combust. Inst., **37**, pp. 4155–4162.
[31] Nakamura, Y., Yoshimura, N., Matsumura, T., Ito, H., and Fujita, O., 2008, "Flame Spread Over Polymer-Insulated Wire in Sub-atmospheric Pressure: Similarity to Microgravity Phenomena," *Progress in Scale Modeling*, Springer, Dordrecht, pp. 17–27.
[32] Nakamura, Y., Yoshimura, N., Matsumura, T., Ito, H., and Fujita, O., 2008, "Opposed-Wind Effect on Flame Spread of Electric Wire in Sub-Atmospheric Pressure," J. Therm. Sci. Technol., **3**(3), pp. 430–441.
[33] Nakamura, Y., Yoshimura, N., Ito, H., Azumaya, K., and Fujita, O., 2009, "Flame Spread Over Electric Wire in Sub-atmospheric Pressure," Proc. Combust. Inst., **32**(2), pp. 2559–2566.
[34] Takahashi, S., Ito, H., Nakamura, Y., and Fujita, O., 2013, "Effect of Conductor on Spreading Flames Over Wire in Microgravity," Proceedings of 43rd International Conference on Environmental Systems, Vail, CO, July 14–18.
[35] Krose, V. J. A., and Van der smagt, P., 1996, *An Introduction to Neural Networks*, University of Amsterdam, Amsterdam.
[36] Chollet, F., 2015, "Keras," https://keras.io/
[37] Boger, Z., and Guterman, H., 1997, "Knowledge Extraction From Artificial Neural Network Models," in EEE International Conference on Systems, Man, and Cybernetics," Computational Cybernetics and Simulation, Orlando, FL, Oct. 12–15.
[38] Linoff, G. S., and Berry, M. J. A., 1997, *Data Mining Techniques: for Marketing, Sales, and Customer Relationship Management*, John Wiley & Sons, New York.
[39] Blum, A., 1992, *Neural Networks in c++: An Object-Oriented Framework for Building Connectionist Systems*, John Wiley & Sons, New York.
[40] Hinton, G., Srivastava N., and Swersky, K., 2012, "Neural Networks for Machine Learning—Overview of Mini-Batch Gradient Descent," http://www.cs.toronto.edu/~hinton/coursera/lecture6/lec6.pdf
[41] Fernandez-Pello, A. C., and Mao, C. P., 1981, "A Unified Analysis of Concurrent Modes of Flame Spread," Combust. Sci. Technol., **26**(3–4), pp. 147–156.